10th International Conference on Fracture Mechanics of Concrete and Concrete Structures
FraMCoS-X
G. Pijaudier-Cabot, P. Grassl and C. La Borderie (Eds)
https://doi.org/10.21012/FC10.236339

ANALYTICAL SOLUTION FOR FRACTURE ANALYSIS OF LIGHTLY REINFORCED CONCRETE BEAMS CONSIDERING BOND-SLIP EFFECT

ZHIMIN WU[*], YANJIE WANG[†] AND YANG LIU[††]

[*]State Key Laboratory of Coastal and Offshore Engineering, Dalian University of Technology,
116024 Dalian, PR China
e-mail: wuzhimin@dlut.edu.cn

[†]State Key Laboratory of Coastal and Offshore Engineering, Dalian University of Technology,
116024 Dalian, PR China
e-mail: yanjiewang1105@mail.dlut.edu.cn

[††]State Key Laboratory of Coastal and Offshore Engineering, Dalian University of Technology,
116024 Dalian, PR China
e-mail: m15641175575@163.com

Key words: Lightly RC beams; Crack propagation; Steel-concrete interface; Bond-slip effect; Analytical solution.

Abstract: Fracture mechanics-based models have been widely used to predict the cracking process of lightly steel-RC beams but the bond behavior of steel-concrete interface has not been evaluated nor its influence on the crack propagation. In this paper, an analytical solution considering bond-slip effect of steel-concrete interface is proposed for modeling the Mode I crack propagation process in lightly RC beams subjected to three-point bending. Based on the classical tri-linear bond-slip model, the full-range interfacial bond behavior is described by five consecutive stages accounting for the local damaging process of the steel-concrete interface that extends with the increase of shear slip. Afterwards, the stress intensity factors (SIFs) induced by the steel force, cohesive force, and the applied load are calculated with the weight function by adopting the *K*-superposition method. Finally, an overall computational equation in terms of a single unknown is derived. Through comparison with the existing test results, it is indicated that the predicted *P*-CMOD curves and peak loads show a good agreement with the test results. Therefore, it can be concluded that the present solution considering bond-slip effect can be effectively used to predict the cracking behavior of lightly RC beams.

1 INTRODUCTION

Fracture behavior of steel-RC beams have drawn much attention as the presence of reinforcing steel affects the crack propagation and modifies the mechanical response. The fracture process in concrete is associated with crack generation, stable and unstable crack extension, and steel-concrete interaction [1]. To better understand the cracking process in RC beams, the bond behavior at the steel- concrete interface needs to be fully understood [2].

Over the last decades, despite extensive studies on the predictions of the crack extension process and reinforcement crack bridging force in RC beams, the slip between the anchor and concrete is often ignored by assuming perfect bond of the steel-concrete interface [3], which is unrealistic when the crack propagates through the reinforced zone [4].

In existing analytical studies, e.g. [5], a assumption of plane sections remain plane is utilized which is invalid when the relative slip occurs at the steel-concrete interface. Against this background, this paper presents an analytical solution to predict the mode-I crack extension process of lightly RC beams, taken into account the bond-slip process involving

various debonding stages.

2 ASSUMPTIONS AND GOVERNING EQUATIONS

2.1 Assumptions

Fig. 1 shows a notched lightly steel-RC beam loaded under three-point bending.

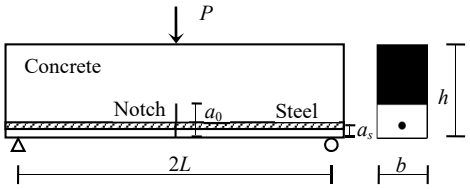

Figure 1: A notched lightly RC beam.

Where b, h, and $2L$ are the beam width, depth, and span, respectively; a_s is the concrete cover thickness, and P denotes the applied load. Before analytical derivation, the basic assumptions are as follows

(1) A single vertical crack with the performed crack length a_0 propagates upward;
(2) The stress-strain relation of steel is shown in Fig. 2, where σ_s and ε_s are the tensile stress and tensile strain of steel; f_y is the yielding strength;
(3) A softening curve depicted in Fig. 3 is utilized to simulate the relation between the cohesive stress σ_w and the crack opening displacement (COD) w, where $w_1 = G_F / f_t$, $w_0 = 5G_F / f_t$, G_F and f_t are the fracture energy and tensile strength of concrete;
(4) A tri-linear bond-slip model is adopted here for representing the relationship between the shear stress τ and the shear slip δ of steel-concrete interface, as shown in Fig. 4, which can be expressed as:

$$\tau = \begin{cases} \dfrac{\tau_u}{\delta_1}\delta \\ \dfrac{-(\tau_u - \tau_r)\delta + \tau_u\delta_2 - \tau_r\delta_1}{\delta_2 - \delta_1} \\ \tau_r \end{cases} \quad (1)$$

Where τ_u and τ_r are the peak and frictional shear stresses of steel-concrete interface; δ_1 and δ_2 are the slip at τ_u and τ_r, respectively.

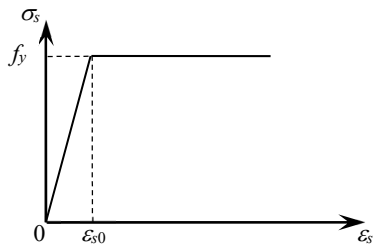

Figure 2: Relationship between tensile stress and strain of reinforced steel bar.

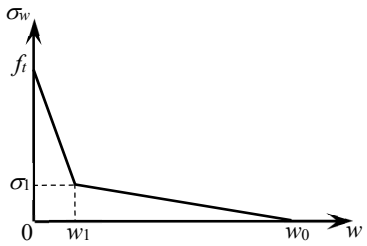

Figure 3: Bilinear softening law of concrete.

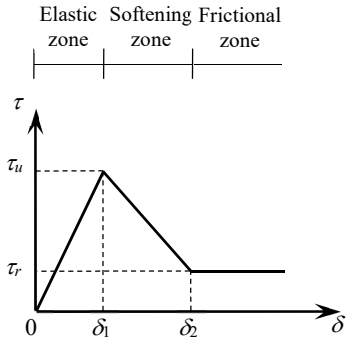

Figure 4: Bond-slip model of steel-concrete interface.

2.2 Governing equation

The left part of the beam is considered (see Fig. 5), where $F(L)$ is the steel force at the mid span. Consider a beam element over dx, the equilibrium equation is

$$\frac{\mathrm{d}\sigma_s}{\mathrm{d}x} = \frac{4\tau}{d_0} \quad (2)$$

Where $\sigma_s(x)$ and d_0 are the tensile stress and the diameter of the steel. Substituting $\sigma_s(x) = E_s\varepsilon_s(x)$ and $\varepsilon_s = \mathrm{d}u_s/\mathrm{d}x$ into Eq. (2) yields

$$\frac{\mathrm{d}^2u_s}{\mathrm{d}x^2} = \frac{4\tau}{E_s d_0} \quad (3)$$

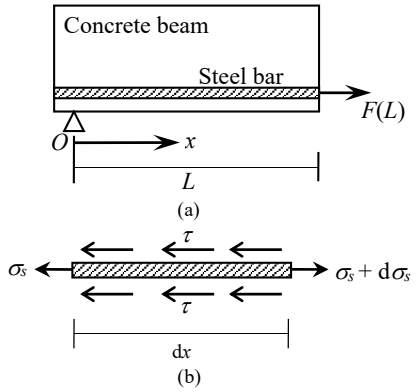

Figure 5: (a) Left part of beam; (b) stress distributions in an element dx of steel.

Where E_s and u_s are the elastic modulus and displacement of steel. The shear slip δ can be written as: $\delta = u_s - u_c$, where u_c is the concrete displacement. Since this paper concerns with a lightly RC beam with a single crack propagated, the concrete displacement u_c is much smaller than the steel displacement u_s as the concrete is much stiffer than the steel. The slip is hence governed by u_s such that the change in u_c has little effect on the results. Thus, u_c is assumed to be constant which can simplify the formulas without loss of accuracy. Eq. (3) is rewritten as

$$\frac{\mathrm{d}^2\delta}{\mathrm{d}x^2} = \frac{4\tau}{E_s d_0} \tag{4}$$

Inserting Eq. (1) into Eq. (4) gives the governing equations

$$\frac{\mathrm{d}^2\delta}{\mathrm{d}x^2} = \begin{cases} \alpha_1^2\delta & \text{(a)} \\ \dfrac{4(\tau_u\delta_2 - \tau_r\delta_1)}{E_s d_0(\delta_2 - \delta_1)} - \alpha_2^2\delta & \text{(b)} \\ \alpha_3\tau_r & \text{(c)} \end{cases} \tag{5}$$

Where (a), (b), and (c) are the elastic, softening, and frictional zones, respectively, and

$$\alpha_1 = \sqrt{\frac{4\tau_u}{E_s d_0 \delta_1}},\ \alpha_3 = \frac{4}{E_s d_0}$$
$$\alpha_2 = \sqrt{\frac{4\tau_u(\tau_u - \tau_r)}{E_s d_0(\delta_2 - \delta_1)}} \tag{6}$$

3 ANALYTICAL SOLUTIONS

3.1 Debonding process of the steel-concrete interface

Using the governing equations described previously, the analytical solutions for the debonding process of the steel-concrete interface can be obtained by imposing the boundary condition at $x = 0$, $\sigma_s(0) = 0$, the boundary condition at $x = L$, $\sigma_s(L) = 4F(L)/\pi d_0^2$, and the continutiy conditions in each loading stage.

(1) Elastic stage. The interface is in an elastic state when the the slip $\delta(L)$ is less than δ_1. For simplicity, only the solution for the steel force is given in the present analysis, i.e.,

$$F(L) = \frac{1}{4}\pi d_0^2 E_s \alpha_1 \tanh(\alpha_1 L)\delta(L) \tag{7}$$

(2) Elastic-softening stage. If the slip $\delta(L)$ is larger than δ_1, the interface consists of the elastic and softening branches. In this stage, the softening length L_s increases while the elastic length L_e decreases. The steel force and the slip can be expressed as

$$\begin{aligned} \delta(L) &= (\delta_1 - \frac{\tau_u\delta_2 - \tau_r\delta_1}{\tau_u - \tau_r})\cos(\alpha_2 L_s) + \frac{\alpha_1\delta_1}{\alpha_2} \\ &\quad \cdot\tanh(\alpha_1 L_e)\sin(\alpha_2 L_s) + \frac{\tau_u\delta_2 - \tau_r\delta_1}{\tau_u - \tau_r} \\ F(L) &= \frac{\pi d_0^2}{4}\Big\{\alpha_2\sin(\alpha_2 L_s)(\frac{\tau_u\delta_2 - \tau_r\delta_1}{\tau_u - \tau_r} \\ &\quad -\delta_1) + \alpha_1\delta_1\tanh(\alpha_1 L_e)\cos(\alpha_2 L_s)\Big\} \end{aligned} \tag{8}$$

(3) Elastic-softening-debonding stage. This stage appears once $\delta(L)$ reaches δ_2. If the frictional length is L_f, $F(L)$ and $\delta(L)$ can be obtained as

The relation between L_e and L_s is

$$\begin{aligned} &\left(\delta_1 - \frac{\tau_u\delta_2 - \tau_r\delta_1}{\tau_u - \tau_r}\right)\cos(\alpha_2 L_s) + \frac{\alpha_1\delta_1}{\alpha_2} \\ &\cdot\tanh(\alpha_2 L_e)\sin(\alpha_2 L_s) = \delta_2 - \frac{\tau_u\delta_2 - \tau_r\delta_1}{\tau_u - \tau_r} \end{aligned} \tag{10}$$

(4) Softening-frictional stage. This stage starts when $\delta(L)$ reaches δ_2. The slip and the steel force are

$$\delta(L)=\delta_2+\frac{\alpha_3\tau_r}{2}L_f^2+ L_f\left[\begin{array}{l}\alpha_2\left(\frac{\tau_u\delta_2-\tau_r\delta_1}{\tau_u-\tau_r}-\delta_1\right)\sin(\alpha_2L_s)\\ +\alpha_1\delta_1\tanh(\alpha_1L_e)\cos(\alpha_2L_s)\end{array}\right]$$

$$F(L)=\pi d_0\tau_rL_f+\frac{1}{4}E_s\pi d_0^2 \cdot\left[\begin{array}{l}\alpha_2\left(\frac{\tau_u\delta_2-\tau_r\delta_1}{\tau_u-\tau_r}-\delta_1\right)\sin(\alpha_2L_s)+\\ \alpha_1\delta_1\tanh(\alpha_1L_e)\cos(\alpha_2L_s)\end{array}\right] \quad (9)$$

$$\delta(L)=\delta_2+\alpha_2\left(\frac{\tau_u\delta_2-\tau_r\delta_1}{\tau_u-\tau_r}-\delta_2\right)\cdot\tan(\alpha_2L_s)L_f+\frac{2\tau_r}{E_sd_0}L_f^2$$

$$F(L)=\pi d_0\tau_rL_f+\frac{1}{4}E_s\pi d_0^2 \cdot\left[\begin{array}{l}\alpha_2\left(\frac{\tau_u\delta_2-\tau_r\delta_1}{\tau_u-\tau_r}-\delta_1\right)\sin(\alpha_2L_s)+\\ \alpha_1\delta_1\tanh(\alpha_1L_e)\cos(\alpha_2L_s)\end{array}\right] \quad (11)$$

(5) Frictional stage. In this stage, the interface is in a friction state. The solutions are as follows

$$\delta(L)=\alpha_3L^2+\delta(0)$$
$$F(L)=2\alpha_3E_sL \quad (12)$$

Based on the above solutions on the entire debonding process, the steel force $F(L)$ can be expressed by

$$F(L)=\psi[\delta(L)] \quad (13)$$

Where the symbol $\psi(\,)$ indicates the relationship between $F(L)$ and $\delta(L)$ at various debonding stages. For lightly RC beams, the steel yielding may occur when $\sigma_S(L)$ increases to the yielding strength f_y. Afterwards, $F(L)$ keeps constant as δ increases, i.e.,

$$F(L)=\frac{1}{4}\pi d_0^2f_y \quad (14)$$

3.2 Analysis of crack extension process in concrete

Based on the *K*-superposition method [6], the stress intensity factor (SIF) at the crack tip is the sum of the SIF provided by the load, K_P, the SIF provided by the cohesive stresses, K_C, and the SIF induced by the steel force, K_S. With the principle of fracture mechanics, the crack propagates once the sum of SIF at the crack tip vanishes, i.e.,

$$Pk_P(a)-K_C(a)-F(L)k_S(a)=0 \quad (15)$$

Where a is the crack length, $k_P(a)$ and $k_S(a)$ denote the SIFs induced by unit applied load and steel force, respectively. In a similar manner, the equation with regard to the crack opening displacement (COD) at the location of steel (i.e., distance of a_s from the crack mouth) w_S is

$$w_s=Pu_P(a_s,a)-U_C(a_s,a) -F(L)u_2(a_s,a) \quad (16)$$

Where $u_P(a_s,a)$ and $u_2(a_s,a)$ are the CODs at the location of the steel caused by unit applied load and steel force, respectively; $U_C(a_s,a)$ is the COD at the location of the steel induced by the cohesive force.

It can be seen from Eqs. (15) and (16) that, the SIFs and the CODs are required to evaluate the crack propagation process in concrete. In this section, the weight function method is adopted to give a rational closed-form solution for calculating the SIFs and CODs in Eqs. (15) and (16) so as to predict the whole crack propagation process. The stress distributions in the cracked section are shown in Fig. 6.

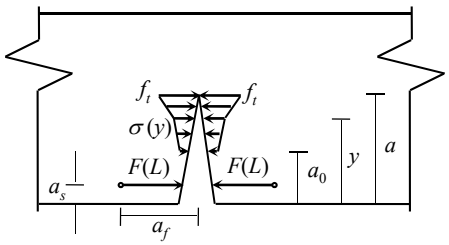

Figure 6: Stress distributions in the cracked section.

The weight function generated by a pair of unit forces can be given in the universal form shown in Eq. (17), where $\beta = y/a$, $\lambda = a/h$, m_1, m_2, m_3, and m_4 are weigh functions [7].

$$m(\beta,\lambda)=\frac{2f(\lambda,\beta)}{\sqrt{\pi a}\sqrt{(1-\lambda)^3}\sqrt{(1-\beta)^2}}$$

$$f(\lambda,\beta)=m_1(\lambda)+\beta m_2(\lambda)+\beta^2 m_3(\lambda)+\beta^3 m_4(\lambda) \quad (17)$$

Making use of the tensile softening law of concrete, the cohesive stress σ_w can be expressed as

$$\sigma_w=\begin{cases} f_t\left(1-\dfrac{4w}{5w_1}\right) & \text{for } w\le w_1 \\ 0.05f_t\left(5-\dfrac{w}{w_1}\right) & \text{for } w_1<w\le w_0 \end{cases} \quad (18)$$

The stress intensity factors are

$$k_P=\frac{3L}{bh^3}\int_0^a(h-2\xi)m(\xi/a,a/h)\mathrm{d}\xi$$

$$K_C=\int_{a_0}^a\sigma_w m(\xi/a,a/h)\mathrm{d}\xi$$

$$k_S=c_f\frac{m(a_s/a,a/h)}{b} \quad (19)$$

Where c_f = the correction factor, which can be given by [8]

$$c_f=\frac{1-\zeta^2}{1.2943}(1.2943+0.0044\zeta+0.1289\zeta^2+10.89\zeta^3-22.14\zeta^4+10.96\zeta^5) \quad (20)$$

Where $\zeta=(1+a/a_f)^{-1}$, and a_f is the distance from the location of steel force acting on the beam to the mid span, which can be obtained by

$$F(L)a_f=\int_0^L\pi d_0\tau(x)x\mathrm{d}x \quad (21)$$

Similarly, the crack opening displacements can be given as

$$u_P=\frac{2}{E_c}\int_{a_s}^a k_P(\eta)m(a_s/a,\eta/h)\mathrm{d}\eta$$

$$U_C=\frac{2}{E_c}\int_{a_0}^a K_C(\eta)m(a_s/a,\eta/h)\mathrm{d}\eta$$

$$u_2=\frac{2}{E_c}\int_{a_s}^a k_S(\eta)m(a_s/a,\eta/h)\mathrm{d}\eta \quad (22)$$

Where E_c is the elastic modulus of concrete. It is assumed that the COD distributes linearly along the beam height. The steel displacements w_s and the CMOD can be written by

$$w_s=2\delta(L)$$

$$\mathrm{CMOD}=(aw_s)/(a-a_s) \quad (23)$$

The global calculation equation is

$$k_S u_P-k_P u_2=\frac{k_S U_C-u_P K_C+2k_P\delta(L)}{\psi[\delta(L)]} \quad (24)$$

Given a crack length a, the slip $\delta(L)$ can be obtained by Eq. (24). The steel force $F(L)$, the load P, and the CMOD can be derived by Eqs. (13), (16), and (23), respectively. A flow chart for the cracking process is outlined in Fig. 7.

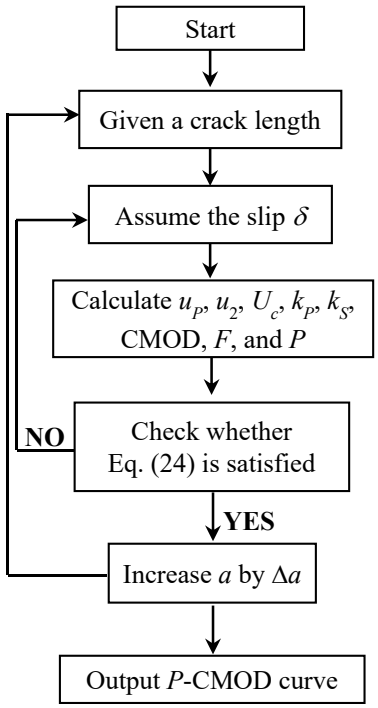

Figure 7: Flowchart of the calculation of the *P*-CMOD curve.

4 VALIDATION

The fracture test on lightly RC beams presented by Yang [9] is used for validation. The measured sizes of each specimen are shown in Table 1, where f_c is the compressive strength of concrete. The span to depth ratio was 0.4. The specimen number 'S153' denoted the specimens with h=150 mm and a_0/h = 0.3. The diameter and yield strength of steel are 6 mm and 503 Mpa for S153, S202 and S203, and 8 mm and 385 MPa for S253 and S303. All beams fail as a result of steel yielding and a certain interfacial slip can be observed.

Table 1: Measured sizes of each specimen

No.	b (mm)	h (mm)	a_0 (mm)	a_s (mm)
S153-1	149	150	44	37
S153-2	149	150	44	35
S153-3	150	151	44	35
S153-4	150	150	44	37
S202-1	149	200	41	33
S202-2	148	201	41	32
S202-3	148	200	41	33
S202-4	148	200	41	34
S203-1	150	200	60	33
S203-2	148	200	58	33
S203-3	147	201	58	28
S203-4	150	200	61	31
S253-1	150	251	76	37
S253-2	148	252	72	31
S253-3	150	250	72	35
S253-4	150	250	72	34
S303-1	151	300	90	40
S303-2	148	300	90	40
S303-3	149	301	90	37
S303-4	148	300	90	38

Table 2: Parameters of test beams

Parameters	Value
E_c (GPa)	26.0
f_c (MPa)	36.0
f_t (MPa)	2.3
E_s (GPa)	210
G_F (N/m)	135
τ_u (MPa)	3.42
δ_1 (mm)	0.21
τ_r (MPa)	3.02
δ_2 (mm)	0.66

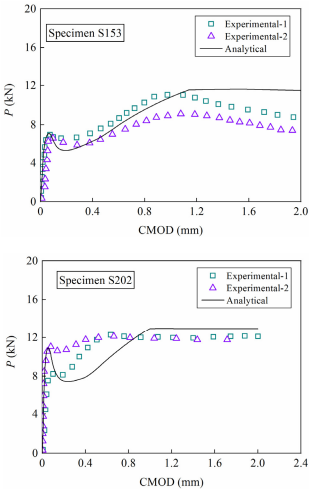

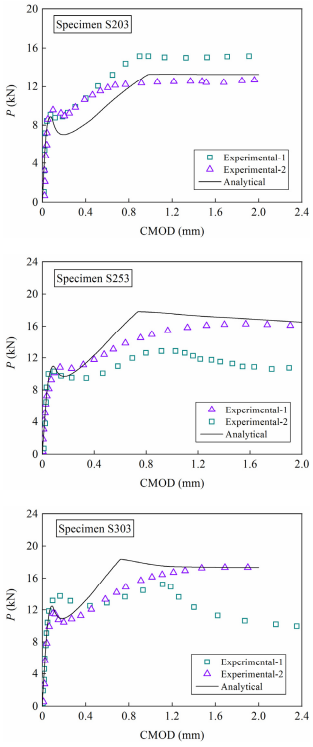

Figure 8: Comparison of P-CMOD curves for each specimen

Table 3: Comparison of P_{1max}

No.	Exp. (kN)	Anal. (kN)	Error (%)
S153-1	—	7.07	—
S153-2	7.01	7.06	0.07
S153-3	—	7.25	—
S153-4	6.78	6.99	3.10
S202-1	8.65	10.52	21.62
S202-2	11.10	10.80	2.70
S202-3	11.06	10.69	3.35
S202-4	—	10.68	—
S203-1	9.48	8.85	6.65
S203-2	—	8.92	—
S203-3	—	9.01	—
S203-4	9.04	8.77	3.25
S253-1	10.59	10.72	1.23
S253-2	—	11.31	—
S253-3	—	11.02	—
S253-4	10.93	11.04	1.01
S303-1	13.73	12.46	9.25
S303-2	—	12.33	—
S303-3	—	12.55	—
S303-4	11.10	12.32	11.00
Average	—	—	5.75

The comparison of *P*-CMOD curves for each specimen is shown in Fig. 8. It can be seen that the analytical predictions are in close agreement with the test results. The predicted P_{1max} and P_{2max} are also compared with the test results, as shown in Tables 3 and 4. It is shown that the predicted peak loads exhibit good agreement with the test results and most of the relative errors between the analytical and test results are below 12%. Specifically, the relative errors are 5.75% for P_{1max} and 8.51% for P_{2max}, which further demonstrates the accuracy of the analytical solution.

Table 4: Comparison of P_{2max}

No.	Exp. (kN)	Anal. (kN)	Error (%)
S153-1	12.99	11.29	13.09
S153-2	11.07	11.35	2.53
S153-3	11.81	11.82	0.08
S153-4	9.13	11.20	22.67
S202-1	12.41	13.01	4.61
S202-2	14.00	13.38	4.63
S202-3	12.18	13.01	8.77
S202-4	12.17	12.74	4.68
S203-1	12.65	12.95	2.37
S203-2	14.70	13.12	11.02
S203-3	16.89	13.69	19.54
S203-4	15.17	13.29	12.39
S253-1	12.79	16.58	29.63
S253-2	17.48	17.09	2.23
S253-3	16.98	16.92	0.35
S253-4	16.21	16.95	4.57
S303-1	15.30	17.02	11.24
S303-2	19.85	17.48	11.94
S303-3	18.19	17.57	3.41
S303-4	17.26	17.32	0.35
Average	—	—	8.51

5 CONCLUSION

This paper presents an analytical solution for the fracture response of lightly RC beams in combination with bond-slip effect at the steel-concrete interface. The validity of the analytical solution is validated by comparing with the test data. The present study can not only be effectively used to predict the crack extension process of lightly RC beams, but also offer insight on the interaction between the cracking behavior of RC beams and the bond behavior of steel-concrete interface.

REFERENCES

[1] Hillerborg, A., Modéer, M., and Petersson, P.E., 1976. Analysis of crack formation and crack growth in concrete by means of fracture mechanics and finite elements. *Cem Concr Res.* 6(6):773-781.

[2] Jason, L., Torre-Casanova, A., Davenne, L., and Pinelli, X., 2013. Cracking behavior of reinforced concrete beams: experiment and simulations on the numerical influence of the steel-concrete bond. *Int J Fract*. 180(2):243-260.

[3] Mi, Z.X., Li, Q.B., Hu, Y., Xu, Q.J., and Shi, J., 2016. An analytical solution for evaluating the effect of steel bars in cracked concrete. *Eng Fract Mech*. 163:381-395.

[4] Ruiz, G., Elices, M., and Planas, J., 1998. Experimental study of fracture of lightly reinforced concrete beams. *Mater Struct*. 31(10):683-691.

[5] Fayyad, T.M. and Lees, J.M., 2018. Integrated fracture-based model formulation for RC crack analysis. *J Struct Eng ASCE*. 144(7):04018083.

[6] Mai, Y.W., 2002. Cohesive zone and crack–resistance (R)-curve of cementitious materials and their fibre-reinforced composites. *Eng Fract Mech*. 69(2):219-234.

[7] Deng, P.R. and Matsumoto, T., 2017. Estimation of the rebar force in RC members from the analysis of the crack mouth opening displacement based on fracture mechanics. *J Adv Concr Technol*. 15(2):81-93.

[8] Zheng, J. J., Dai, J. G., and Fan, X. L. 2015. Fracture Analysis of FRP-Plated Notched Concrete Beams Subjected to Three-point Bending. *J Eng Mech ASCE.* 142(3): 04015096.

[9] Yang, S.T., 2008. Study on mechanical behaviors at tendon-concrete and FRP-concrete interfaces based on fractured mechanics. *Dalian Univ of Technol*. Ph. D. thesis. (in Chinese).